Mesostructured thin films as electrocatalysts with tunable composition and surface morphology

Dennis F. van der Vliet[1][†], Chao Wang[1][†], Dusan Tripkovic[1], Dusan Strmcnik[1], Xiao Feng Zhang[2], Mark K. Debe[3], Radoslav T. Atanasoski[3], Nenad M. Markovic[1] and Vojislav R. Stamenkovic[1]*

Among the most challenging issues in technologies for electrochemical energy conversion are the insufficient activity of the catalysts for the oxygen reduction reaction, catalyst degradation and carbon-support corrosion. In an effort to address these barriers, we aimed towards carbon-free multi/bimetallic materials in the form of mesostructured thin films with tailored physical properties. We present here a new class of metallic materials with tunable near-surface composition, morphology and structure that have led to greatly improved affinity for the electrochemical reduction of oxygen. The level of activity for the oxygen reduction reaction established on mesostructured thin-film catalysts exceeds the highest value reported for bulk polycrystalline Pt bimetallic alloys, and is 20-fold more active than the present state-of-the-art Pt/C nanoscale catalyst.

Over the past decades, extensive research has been devoted to the development of technologies that can effectively convert energy and become economically viable for use by the general public. Great expectations are held for technologies such as fuel cells and lithium–air batteries that rely on electrochemical processes. In both cases, satisfactory energy density can be attained; however, a major challenge lies in the insufficient activity and durability of the materials that are employed at present as cathode catalysts for electrochemical reduction of oxygen. These limitations inevitably lead to a lower operating efficiency of the devices, which highlights the need for the development of more active and durable oxygen reduction reaction (ORR) catalysts[1–12]. In the case of fuel cells, most of the research centres on platinum, the best monometallic catalyst for the ORR. At the present state of development, an approximately fivefold reduction in Pt content is necessary to meet cost requirements for large-scale automotive applications[5]. Pt-based alloys have already made an impact in fuel-cell catalyst design by decreasing the amount of platinum while improving activity and durability[12–18], which places these materials at the focus of intensive fundamental and applied research on both extended (bulk)[17–25] and nanoscale systems[7,14–16,26–34]. The main challenge in that effort is linked to the possibility of achieving the unique structural and compositional profile of the Pt$_3$Ni(111) alloy, which was established from single-crystal studies[12,17]. Such a profile was obtained on extended surfaces by thermal annealing that facilitates thermodynamically driven segregation of Pt to form a pure ordered surface layer, denoted as Pt(111)-skin. The electronic structure of Pt(111)-skin is altered by the subsurface layer of PtNi (in 1:1 ratio) and is responsible for the extreme ORR activity, which is nearly two orders of magnitude higher than the state-of-the-art Pt/C catalyst. Consequently, the ability to mimic the compositional profile and structure of Pt-skin in high-surface-area catalysts would bring unprecedented benefits to technologies that rely on the ORR. However, despite numerous attempts, this goal has not been achieved yet for practical catalysts.

Here we present a new class of materials based on mesostructured multimetallic thin films with adjustable structure and composition, which have been tailored to emulate the distinctive properties of the Pt(111)-skin, to be employed in electrochemical devices. The design of these materials relied on our previous work related to well-defined extended and nanoscale surfaces in the form of PtM alloys (M = Ni, Co, Fe, V, Ti; refs 17–20). We aimed towards catalysts that can bridge the world of extended surfaces with superior activity and nanoscale systems with high specific surface area, to harvest maximal utilization of precious metals. Such synergy is foreseen to be present at the mesoscale, which implies not only a specific length scale, but rather a principle of operating in between different physical regimes that exhibit distinct functional behaviour[35]. Considering that mesoscale materials chemistry is still in its infancy, it is expected that this field will open pathways in materials design that arise from the rational control of physico-chemical properties and functionality of mesostructured systems. In particular, for electrocatalytic materials, most previous work has emphasized either achievement of high surface area through small particle size, or the attainment of a better understanding of fundamental properties through the use of extended surfaces. From such studies, it is well known that there are substantial differences in catalytic properties between nanoscale and bulk materials. The benefits of targeting mesoscale architectures between these extremes have scarcely been explored, especially in the sense of transferring superior characteristics from extended surfaces to practical materials. In view of that, instead of using discrete nanoparticles (3–5 nm) supported on high-surface-area carbon[26–28,32–34,36], we deployed continuous Pt and Pt-alloy nanostructured thin films[29,37–41] (NSTF) over an oriented array of molecular solid whiskers by physical vapour deposition. Specifically, planar magnetron sputter deposition was used to deposit thin metal films with a wide range in composition. Such NSTF catalysts provide good surface area utilization and eliminate issues related to carbon-support corrosion and contact resistance at the carbon/metal interface that would lead to poor utilization and degradation of the catalyst[14]. The capability to control the deposition rate, as well as the combination and order of constituents, signifies sputter deposition as an effective tool to form thin films with desirable thickness, composition profile
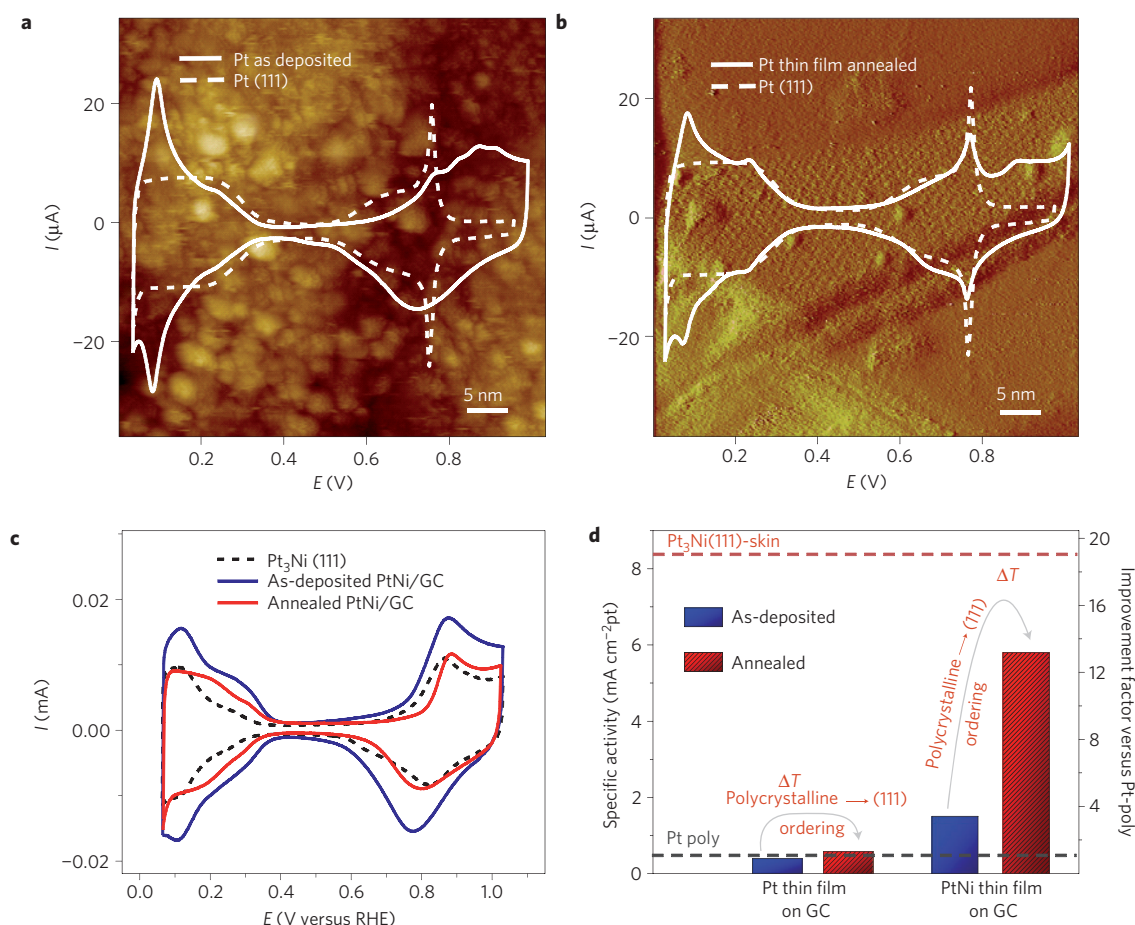
Figure 1 | CV and STM images of Pt and Pt alloy 20-nm thin films deposited on a glassy carbon substrate. a, As-deposited Pt thin film (solid line) and Pt(111) (dashed line). **b**, Annealed Pt thin film (solid line) and Pt(111) (dashed line). **c**, CV profile of as-deposited (blue line), annealed PtNi thin film (red line) and Pt$_3$Ni(111)-skin (dashed line). **d**, Specific activities measured by RDE in 0.1 M HClO$_4$ with 1,600 rpm, 20 mV s^{-1} at 0.95 V with corresponding improvements factors versus polycrystalline Pt.

and surface roughness. However, the surface structure of a thin film, an important catalytic parameter[33,42–44], cannot be altered by this method to match those established on single-crystalline systems. For that reason, we attempted a thorough examination of thin-film properties on extended, flat, non-crystalline and chemically inert substrates such as a mirror-polished glassy carbon surface. This approach brings an extra level of control in terms of defined geometric surface area and surface roughness factor that is unattainable in the case of nanoscale substrates. Consequently, our efforts have been directed towards exploring structural transitions in polycrystalline thin films.

The first step comprised the deposition of a pure Pt thin film onto an ultrahigh-vacuum-cleaned glassy carbon substrate, which was followed by thermal annealing in a reductive atmosphere (see Methods). The morphology of the Pt film was validated by scanning tunnelling microscopy (STM) as shown in Fig. 1a,b. The difference between as-deposited versus annealed Pt films indicates a substantial change in the thin-film surface morphology due to rearrangement of the Pt topmost atoms towards the (111) structure with minimum surface energy. The as-deposited Pt film has a corrugated nanostructured three-dimensional surface morphology with an average grain size of ∼5 nm, whereas the morphology of the annealed thin film has been transformed into a smooth two-dimensional surface with large 20 × 100 nm hexagonal (111) facets. In accordance with the STM results, the characteristic surface features are also confirmed by electrochemical cyclic voltammetry (CV). Figure 1a reveals that the CV profile of the as-deposited thin-film surface

matches the one established for bulk polycrystalline Pt. On the other hand, Fig. 1b shows that the CV profile of the annealed Pt thin film underwent extensive transformation from typical polycrystalline into Pt(111)-like with characteristic fingerprint features between 0.5 and 0.9 V; the so-called butterfly region that corresponds to adsorption/desorption processes of OH$_{ad}$ on Pt(111) facets (see Supplementary Information). Therefore, it is evident from both STM and CV that the annealed extended thin film consists of predominantly (111) facets encompassing the entire surface. In fact, the degree of resemblance in electrochemical signature between the annealed thin-film surface and single-crystal Pt confirms that the (111) facets are both large and interconnected. The synergy between the surface structure, domain size and functionality defines that the thin-film surface has a distinct mesostructured morphology. These findings clearly demonstrate the feasibility of controlling surface ordering of extended Pt thin films deposited over a non-crystalline substrate, that is, without the use of templates for epitaxial growth. Instead of building the crystal lattice from a seed or underlying crystalline substrate, individual randomly oriented nanoscale grains coalesce and form large well-ordered (111) facets. All of that greatly expands the potential for utilization of thin-film materials and introduces thermal annealing in a controlled atmosphere as a compelling tool in the fine tuning of a thin film's structure and hence electrocatalytic properties.

In the following steps we proceed towards a bimetallic PtNi thin film with the same thickness to mimic the composition profile of the Pt$_3$Ni(111) system and to replicate its unique catalytic properties.
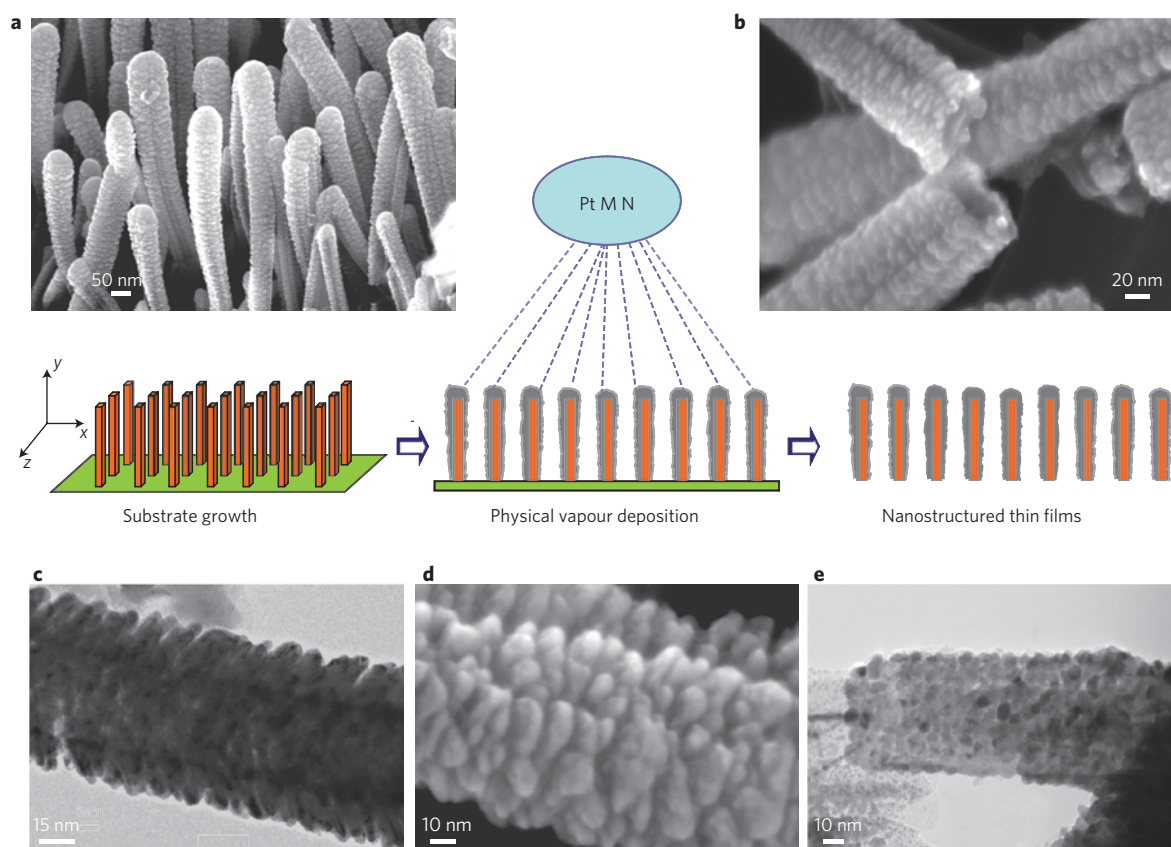
Figure 2 | HRSEM and TEM micrographs of the NSTF whiskers. Centre: schematic illustration of the vacuum protocol that has been used for the growth of aligned perylene red substrate, which is then coated by a metallic thin film with an adjustable thickness and composition profile (Pt; M and/or N = Ni, Co, Fe, Ti, V). **a**, HRSEM snapshot of a group of whiskers that indicates their length, shape and alignment after thin-film deposition. **b**, HRSEM close-up of an intentionally broken single whisker that demonstrates the thickness of the metallic film over perylene red substrate. **c**, HRTEM close-up of a single whisker side, which reveals growth of whiskerettes along the whisker. **d**, HRSEM insight into the whisker's surface showing a close-packed formation of whiskerette tips of 5 nm in diameter that facilitates a highly corrugated morphology. **e**, TEM micrograph of a whisker side that confirms the grained texture of the sputtered thin film and the average diameter of the whiskerettes.

The results from the electrochemical measurements in Fig. 1c,d confirm that as for monometallic Pt, the polycrystalline nature of the as-deposited alloy thin film is predominantly transformed into a Pt(111)-skin-like surface. This is obvious from both the CV profile of the annealed alloy thin film that resembles the one obtained on Pt₃Ni(111) and its superior catalytic activity for the ORR, which was up to now obtained exclusively on the Pt₃Ni(111)-skin surface[17,45]. The combination of the Pt(111)-skin-like voltammetry and the marked increase in the ORR activity proves that surface ordering from randomly oriented towards (111) is indeed feasible for bimetallic thin films, and demonstrates that the catalytic improvement obeys the same mechanism as previously reported for Pt-bimetallic single-crystal surfaces; that is, electronic modification of the topmost Pt layer leads to extreme catalytic enhancement solely for the (111) orientation[19]. Therefore, the ORR-specific activity, which equals 70% of the value established for the most active catalyst, Pt₃Ni(111)-skin, serves as a descriptor that (111)-skin facets are dominating on the annealed thin-film surface. Together this demonstrates the twofold power of annealing in facilitating the formation of the mesostructured alloy thin-film morphology, characterized by both an energetically more favourable surface state rich in (111) facets, and the desired compositional profile.

It is these results that provide the driving force for a shift towards corresponding thin-film-based high-surface-area materials. A Pt-alloy NSTF catalyst is deposited by magnetron sputtering over an array of molecular solid whiskers, composed of an organic pigment N, N-di(3,5-xylyl)perylene-3,4:9,10 bis(dicarboximide); hereafter denoted as perylene red[29,37–39,46]. Figure 2 illustrates the step-by-step deposition process of the thin metal films onto the perylene red support, as well as high-resolution scanning electron microscopy (HRSEM) and transmission electron microscopy (TEM) micrographs of the NSTF whiskers. These images reveal a detailed insight into critical parameters of the NSTF such as metallic film thickness, length, shape and surface morphology. A single whisker measures on average about 800 nm in length, and the film thickness is 5–20 nm. In Fig. 2, it is clearly visible that on the sides of a single whisker, smaller metal alloy whiskerettes are formed with a diameter of ∼5 nm (Fig. 2c), and a close-up of a broken whisker (Fig. 2b) illustrates the metallic film/shell that surrounds the perylene red substrate. Surface-specific HRSEM in Fig. 2b,d unveils that the side walls along the whisker have a very rough surface morphology, consisting mainly of whiskerette tips bonded closely to each other to produce densely packed corncob-like features, providing the validity of terming this material a NSTF. It is important to emphasize that the highly grained texture of the NSTF side walls made of closely packed whiskerettes is also confirmed in the TEM micrograph in Fig. 2e. Such structural parameters greatly affect the functional properties of the NSTF, and therefore the ability to control and tune them along with the near-surface compositional profile can lead towards a substantial gain in catalytic performance.
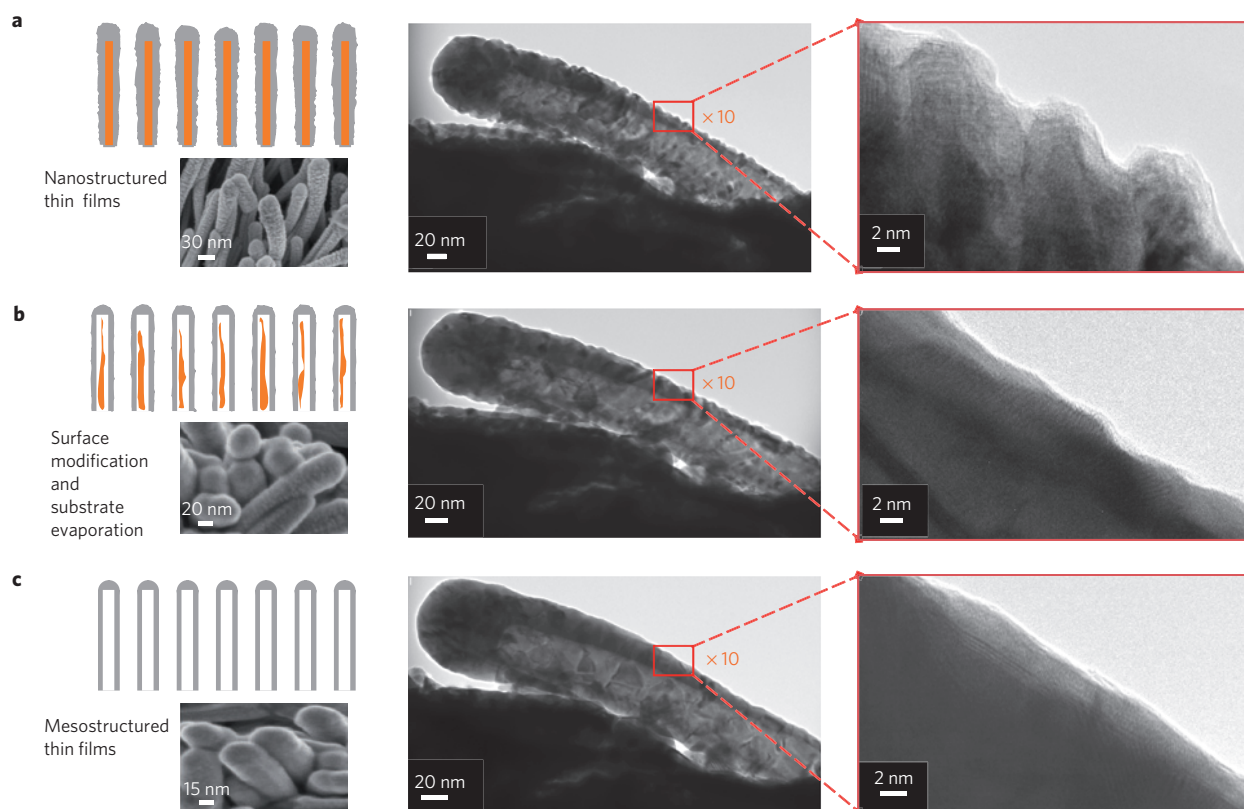
Figure 3 | *In situ* transformation from nanostructured into mesostructured thin film during annealing. a–c, Middle: HRTEM images of progressive annealing between room temperature and 400 °C on a single whisker that capture the ordering from randomly oriented to a homogeneous structure with visible crystalline domains. Right: HRTEM close-up of the transformation for the same near-surface region during annealing, from highly corrugated into a flat and smooth surface morphology. Left: schematic illustration of the mesoscale ordering during annealing and formation of the mesostructured thin film catalyst, associated with the corresponding HRSEM insets.

In what follows, we apply an experimental approach combined with the knowledge related to highly active well-defined single-crystalline and extended thin-film surfaces to develop mesostructured thin-film electrocatalysts with advanced properties. *In situ* HRSEM and TEM are simultaneously employed during NSTF annealing in a controlled atmosphere. This allows us to visualize real-time structural changes at the atomic level and to follow rearrangements of the surface and sub-surface morphology of thin-film materials. This insight is invaluable in the fine-tuning of the materials' properties. Figure 3 depicts *in situ* results obtained during thermal annealing of a single PtNi-NSTF whisker. The NSTF catalyst is mounted onto the HRTEM heating stage and is introduced to a reductive atmosphere of argon and hydrogen gases. As the specimen is gradually heated, no change in surface morphology is observed as depicted in Fig. 3a, which reveals the initial stage and a close-up of the grained highly corrugated whisker side wall and its surface. Once the temperature reaches 300 °C, we start to follow real-time restructuring of the thin film's morphology. Figure 3b captures the onset of the surface transformation, which appears as a smoothening of the near-surface regions. The steady-state structure is achieved after 30 min and is shown in Fig. 3c. These images illustrate that the densely packed organization with the initial three-dimensional surface morphology is being transformed into a more homogeneous, flat and ordered two-dimensional thin-film material with clearly observable crystalline features in its walls. This thermodynamically driven transition releases stress and strain of the as-deposited thin film and leads towards the state with minimum surface energy without compromising the overall shape and dimension of the whisker. As for Pt thin films on glassy carbon, the initial nanostructured surface morphology that originated from

the closely bonded whiskerettes' tips is transformed into a smooth continuous film with large crystalline domains (20–40 nm). Specifically, randomly oriented nanoscale grains coalesce and give rise to a mesostructured thin film with unique physicochemical properties; therefore, the materials after this treatment will be referred to as mesostructured thin films (Meso-TF). Close inspection of HRTEM micrographs after applied thermal treatment (see Supplementary Information) confirms that emerged facets with (111) structure prevail on the surface whereas undercoordinated sites are diminished, which also has important implications towards improved stability. As a side effect, the perylene red substrate is removed during this procedure (details can be found in the Supplementary Information). In addition to HRTEM/SEM studies, X-ray diffraction measurements, which show enhanced alloying and an increase in the number of (111)-oriented domains on the Meso-TF, are presented in the Supplementary Information.

The final step in the characterization is to obtain the electrochemical signature and compare adsorption and catalytic properties between different classes of thin-film materials and the state-of-the-art Pt/C catalyst by rotating-disc electrode (RDE), see Methods section. As expected, from the CV profile depicted in Fig. 4 we find that the smooth morphology of the Meso-TF slightly lowers the electrochemically active surface area (ECSA), from $\sim$11 m^2 g^{-1} for the NSTF to $\sim$9 m^{2}g$_{Pt}^{-1}$ for the Meso-TF. This implies that most of the inner portion of the whiskers, which has been vacated by the perylene red, is not electrochemically active, presumably owing to lack of penetration of the electrolyte into the hollow of the whisker (see closed whisker end in Fig. 3). As shown in Fig. 4a, the CV profile of PtNi NSTF whiskers exhibits similar behaviour to monometallic Pt NSTF with clearly visible polycrystalline Pt features due to
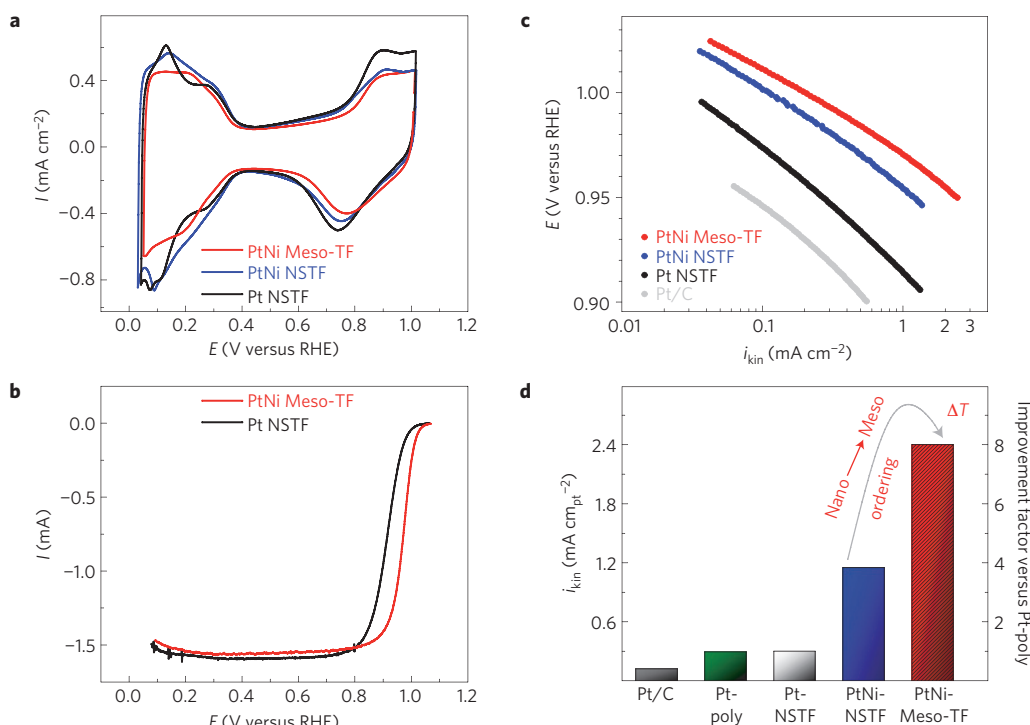
Figure 4 | CV on the Pt-based thin-film catalysts. a, Cyclic voltammograms of Pt-NSTF, PtNi-NSTF and PtNi-Meso-TF. **b**, The ORR polarization curves. **c**, Corresponding Tafel plots (Tafel slopes are determined at potentials higher than the half-wave potential ($E_{1/2}$; potential at which $I = 1/2\ I_{diff}$), to avoid diffusion- and solution-resistance-induced errors). **d**, Specific activities measured at 0.95 V and improvement factor versus Pt-poly (and Pt-NSTF).

the adsorption–desorption processes of underpotentially deposited hydrogen (H_{upd}). However, the H_{upd} region of PtNi Meso-TF is significantly different with a characteristic flat plateau (Fig. 4a), which confirms that the surface has a relatively large contribution of (111) facets compared with the highly corrugated sputtered thin film that is rich in low-coordinated Pt sites. This is also in good agreement with HRTEM and X-ray diffraction results. Moreover, the onset of surface oxide formation is shifted positively in the following order: Pt-NSTF < PtNi-NSTF < PtNi Meso-TF. Accordingly, the ORR polarization curves, shown in Fig. 4b, follow the same trend in activity. Figure 4c and Fig. 4d summarize the kinetic current densities (specific activities per ECSA of Pt) as Tafel plots and a bar graph, respectively. As specific activity is a fundamental property of a material that reflects its intrinsic catalytic performance, as opposed to mass activity, which emphasizes the optimized dispersion of a material, our focus has been placed on boosting specific activity. This approach leads to a higher turnover frequency (the measure of activity per active site), which may result in better utilization of Pt, culminating in higher mass activity. Considering the large increase in specific activity, we report values measured at 0.95 V to avoid diffusion-induced errors in kinetic current densities. The order of specific activity becomes apparent, with Pt/C being the least active, followed by Pt-NSTF and polycrystalline Pt. One can observe a significant increase in activity for PtNi Meso-TF, accompanied by a decrease in Tafel slope from ∼70 mV dec^{-1} for monometallic Pt to ∼40 mV dec^{-1}. This value is considerably lower than those commonly reported for Pt-based catalysts in the literature[19,47], but it is in line with the value obtained on Pt$_3$Ni(111)-skin[47]. The activity of PtNi Meso-TF exhibits an improvement factor of over 8 versus Pt-poly and Pt-NSTF. Furthermore, when compared with the state-of-the-art conventional Pt/C catalyst, the specific activity of the PtNi Meso-TF achieves an unprecedented 20-fold enhancement. Even though optimal film thickness, alloy composition and total Pt loading will be extensively studied in the future, the measured improvement

expressed in A/mg$_{Pt}$ corresponds to a mass activity that is already three times higher than the US Department of Energy technical target[12]. Together, the flat voltammetric curves, the trend in specific activity, the low Tafel slope and the structural characterizations strongly suggest that the annealed PtNi Meso-TF has a Pt-skin-type near-surface structure.

To review the findings on thin-film-based mesostructured catalysts and to merge them into the same chart with nanoscale systems and bulk materials, we present in Fig. 5 the ORR activity map for different classes of Pt alloys, that is, from nanoparticles dispersed on high-surface-area carbon, to polycrystalline bulk materials and to single-crystalline alloys of Pt$_3$Ni(hkl) surfaces[19]. This map shows a huge span in intrinsic specific activities among materials of the same bulk elemental composition that differ in form and surface structure. It also demonstrates the importance of controlling fundamental properties that determine catalytic performance; specifically that the ability to alter physical parameters such as particle size, near-surface composition profile, morphology and surface structure can lead to great improvements in functional properties of real catalysts. Notably, we have explored a number of NSTF catalysts with different compositions as summarized in Fig. 5; however, for the sake of brevity in this report we have presented only the results for the PtNi in detail. The activity values are given for Pt alloys with different transition metals associated with the atomic number (Z). The main features in Fig. 5 are designated activity regions for different classes of materials. Metallic nanoparticles of Pt and Pt alloys dispersed on a high-surface-area carbon support exhibit profoundly lower activities compared with their polycrystalline bulk counterparts. The assigned region that reflects the activity range of metallic nanoparticles is based on the literature data reported for Pt-alloys obtained by conventional impregnation methods. The next level in activity is reserved for extended bulk polycrystalline systems, where the specific activity of Pt$_3$M-alloys can be improved by a factor of three versus Pt-poly. As mentioned above, the capability to control the surface
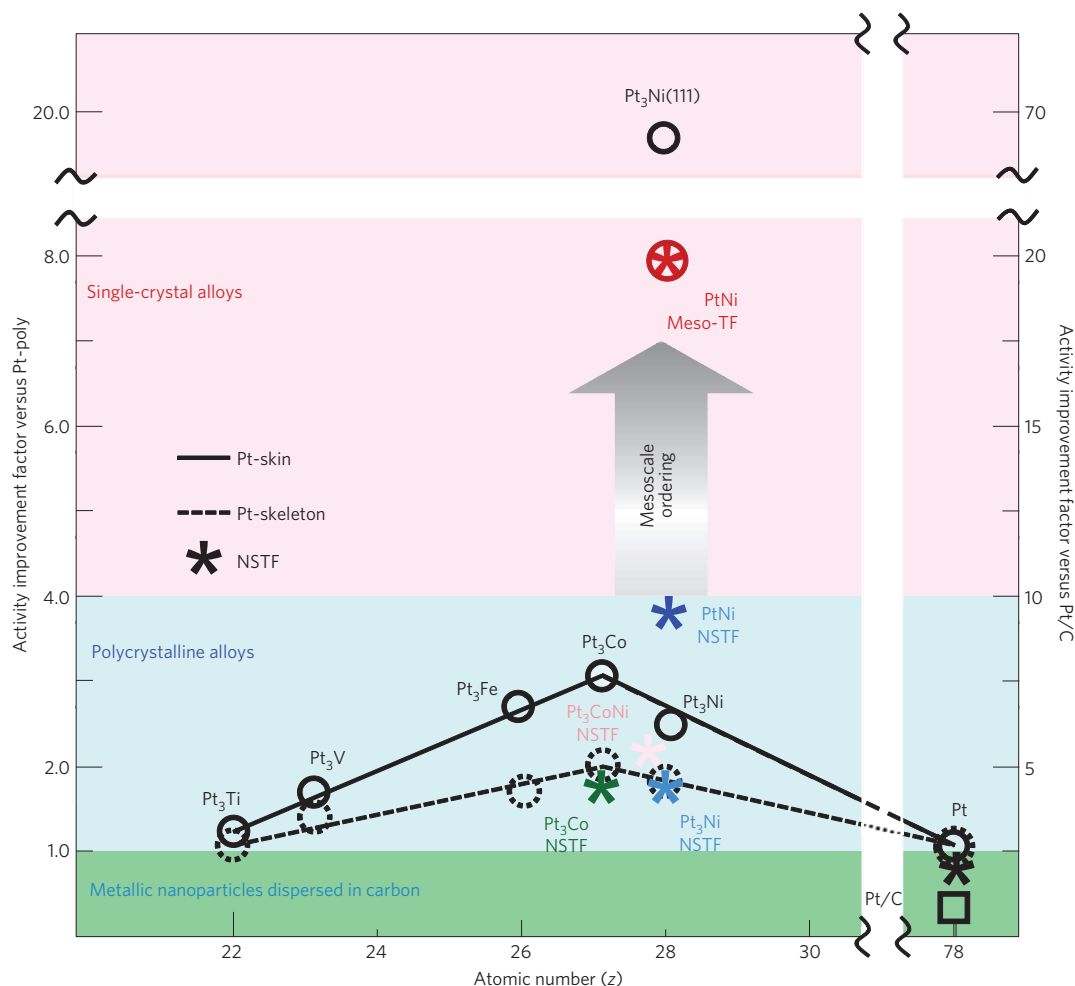
Figure 5 | Activity map for the ORR obtained for different classes of Pt-based materials. Improvement factors are given on the basis of activities compared with the values for polycrystalline Pt and the state-of-the-art Pt/C catalyst established by RDE measurements in 0.1 M HClO₄ at 0.95 V.

structure leads to an extra boost in activity, and hence the highest ORR activity ever measured was obtained for the Pt₃Ni(111)-skin surface. On the basis of the values depicted in Fig. 5, the NSTF catalysts can successfully mimic the catalytic behaviour of polycrystalline bulk materials, while Pt-alloy mesostructured thin films exceed the range designated for polycrystalline systems. This is the first practical catalyst to approach the levels of activity previously reserved only for bulk single-crystalline surfaces, owing to the formation of a surface and near-surface structure similar to that of the ideal Pt₃Ni(111)-skin. These bimetallic Meso-TF materials preserve sufficiently high specific surface area, which enables better utilization of precious metals. Moreover, Pt-based catalysts with mesoscale features also avoid the activity losses that are caused by the higher fraction of low-coordinated surface atoms that are present in nanoscale catalysts[14]. Consequently, thin-film electrocatalysts are hampered neither by the stability issues that accompany the use of high-surface-area carbon support, nor by the loss of active surface area due to particle agglomeration. The mesostructured thin films, therefore, unite the beneficial properties of both the nanoscale and the extended bulk systems, and lead to new design rules for producing highly active and durable electrocatalysts. These findings provide a proof of concept that the ability to tailor the composition, morphology and structure of the thin-film-based materials at the mesoscale allows the harvesting of maximal performance from the employed constituents. This is a seeding study on mesoscale ordering in electrocatalysts where further advancement towards an increased presence of (111) facets

and optimization of the thin-film thickness may lead to additional improvements in specific and mass activities.

We report on a new class of mesostructured catalysts based on thin films with an adjustable composition profile and surface morphology. These materials are in the form of metallic thin films with properties that have been tailored to improve the activity for the ORR. The obtained ORR activity is the highest ever measured on non-bulk catalysts owing to the beneficial near-surface compositional profile and its highly crystalline surface morphology. The exceptional properties of this Meso-TF are comparable to extended single-crystalline surfaces and improvement factors in kinetic activity of 8 versus polycrystalline Pt and 20 versus Pt/C are observed. The substantial advances in catalytic performance are obtained through structural mesoscale ordering of the thin film induced by thermal annealing in a reductive atmosphere. The approach as developed can be applied to generate a wide range of (electro)catalysts with tailored structure/composition, ultralow precious metal content and superior functional properties such as activity and durability.

Methods

Thin-film deposition. Thin metal films were deposited by planar magnetron sputter deposition on the ultrahigh-vacuum-cleaned surface of a mirror-polished glassy carbon substrate of 6 mm in diameter (base vacuum 1×10^{-10} torr). The deposition rate was set to 0.3 Å s⁻¹ by a quartz-crystal microbalance and an exposure of 7 s was calibrated for the nominal thickness of 2.2 ~ 2.3 Å for a monolayer of Pt. The film thickness was derived from the exposure time of computer-controlled shutters during deposition. The thickness of all thin films in

this study was 20 nm. In the case of NSTF catalysts, consecutive layers of platinum and the metal of choice were deposited onto the NSTF layer of oriented organic pigment (perylene red) whiskers also by planar magnetron sputter deposition in vacuum[48]. The deposition process covered each of the perylene red whiskers with a thin metallic film. Both the monometallic Pt and the Pt-alloy catalyst were obtained by this method. The Meso-TF were obtained by thermal annealing of NSTF at 400 °C in a hydrogen-rich atmosphere. The temperature was increased in increments of 20 °C per 5 min and the whole process lasted 2 h.

Electrochemical measurements. An Autolab PGSTAT 30 with FI20, ECD, ADC and SCAN GEN modules was used for the electrochemical measurements. Perchloric acid diluted with MilliQ water to 0.1 M was the electrolyte in all cases. The gases used were research grade (5N5+) argon and oxygen. In all experiments, a silver–silver chloride was the reference electrode. However, all potentials referred to in this paper are converted to the pH-independent reversible hydrogen electrode scale. We repeated all experiments 8 times to confirm reproducibility, and to improve the accuracy in the determination of kinetic activities. Kinetic current densities were obtained from the measured ORR polarization curves in accordance with the Koutecky–Levich equation: $I_{ORR}^{-1} = I_{kinetic}^{-1} + I_{diffusion}^{-1}$. The ECSA of the nanocatalysts was determined by integrating both the H_{upd} part of the CV profile, and the polarization curve obtained by oxidation of a monolayer of adsorbed carbon monoxide to avoid underestimation of the surface area due to altered hydrogen adsorption properties. All catalysts were deposited on a RDE made of glassy carbon and the loading of the nanoscale thin-film catalysts was adjusted to be 60 $\mu g_{Pt}\, cm_{disc}^{-2}$, whereas the loading for Pt/C obtained from TKK was 12 $\mu g_{Pt}\, cm_{disc}^{-2}$. Kinetic current densities as reported are normalized by ECSA in all cases.

Microscopy. A Hitachi H-9500 environmental transmission electron microscope operated at 300 kV was used to perform the microstructural characterization and *in situ* heating TEM study. Powder samples were attached to the heating zone of a Hitachi gas-injection-heating holder. Images of nanoparticles were first recorded at room temperature, followed by heating of the specimen inside the microscope chamber with a vacuum level of about 10^{-4} Pa. A CCD (charged-coupled device) camera was used to monitor the microstructural evolution and record images and videos. Each heating temperature was held for at least 10 min for detailed structural characterization, including morphology and atomic structure. A Hitachi SU70 high-resolution field-emission SEM was used for routine nanoparticle sample inspection. For the detailed surface morphology study at the nanometre scale, a Hitachi S-5500 ultrahigh-resolution cold field-emission SEM delivered a much higher resolution power (0.4 nm secondary electron image resolution at 30 kV) than normal SEM because of the specially designed objective lens. On both SU70 and S-5500, secondary electron images were taken at 15 kV or 30 kV to reveal the surface morphology of both the as-deposited, as well as the annealed nanoparticles.

References

1. Borup, R. *et al.* Scientific aspects of polymer electrolyte fuel cell durability and degradation. *Chem. Rev.* **107**, 3904–3951 (2007).
2. Wagner, F. T., Lakshmanan, B. & Mathias, M. F. Electrochemistry and the future of the automobile. *J. Phys. Chem. Lett.* **1**, 2204–2219 (2010).
3. Adzic, R. R. *et al.* Platinum monolayer fuel cell electrocatalysts. *Top. Catal.* **46**, 249–262 (2007).
4. Bruce, P. G., Freunberger, S. A., Hardwick, L. J. & Tarascon, J. M. Li-O₂ and Li-S batteries with high energy storage. *Nature Mater.* **11**, 19–29 (2012).
5. Gasteiger, H. A., Kocha, S. S., Sompalli, B. & Wagner, F. T. Activity benchmarks and requirements for Pt, Pt-alloy, and non-Pt oxygen reduction catalysts for PEMFCs. *Appl. Catal. B-Environ.* **56**, 9–35 (2005).
6. Arico, A. S., Bruce, P., Scrosati, B., Tarascon, J. M. & Van Schalkwijk, W. Nanostructured materials for advanced energy conversion and storage devices. *Nature Mater.* **4**, 366–377 (2005).
7. Strasser, P. *et al.* Lattice-strain control of the activity in dealloyed core–shell fuel cell catalysts. *Nature Chem.* **2**, 454–460 (2010).
8. Greeley, J. *et al.* Alloys of platinum and early transition metals as oxygen reduction electrocatalysts. *Nature Chem.* **1**, 552–556 (2009).
9. Zhang, J., Sasaki, K., Sutter, E. & Adzic, R. R. Stabilization of platinum oxygen-reduction electrocatalysts using gold clusters. *Science* **315**, 220–222 (2007).
10. Nilekar, A. *et al.* Bimetallic and ternary alloys for improved oxygen reduction catalysis. *Top. Catal.* **46**, 276–284 (2007).
11. Gorlin, Y. & Jaramillo, T. F. A bifunctional nonprecious metal catalyst for oxygen reduction and water oxidation. *J. Am. Chem. Soc.* **132**, 13612–13614 (2010).
12. Debe, M. K. Electrocatalyst approaches and challenges for automotive fuel cells. *Nature* **486**, 43–51 (2012).
13. Snyder, J., Fujita, T., Chen, M. W. & Erlebacher, J. Oxygen reduction in nanoporous metal-ionic liquid composite electrocatalysts. *Nature Mater.* **9**, 904–907 (2010).
14. Wang, C. *et al.* Design and synthesis of bimetallic electrocatalyst with multilayered Pt-skin surfaces. *J. Am. Chem. Soc.* **133**, 14396–14403 (2011).
15. Wang, C. *et al.* Multimetallic Au/FePt₃ nanoparticles as highly durable electrocatalyst. *Nano Lett.* **11**, 919–926 (2010).
16. Ferreira, P. J. *et al.* Instability of Pt/C electrocatalysts in proton exchange membrane fuel cells—A mechanistic investigation. *J. Electrochem. Soc.* **152**, A2256–A2271 (2005).
17. Stamenkovic, V. R. *et al.* Improved oxygen reduction activity on Pt₃Ni(111) via increased surface site availability. *Science* **315**, 493–497 (2007).
18. Stamenkovic, V. R. *et al.* Trends in electrocatalysis on extended and nanoscale Pt-bimetallic alloy surfaces. *Nature Mater.* **6**, 241–247 (2007).
19. Stamenkovic, V., Schmidt, T. J., Ross, P. N. & Markovic, N. M. Surface composition effects in electrocatalysis: Kinetics of oxygen reduction on well-defined Pt₃Ni and Pt₃Co alloy surfaces. *J. Phys. Chem. B* **106**, 11970–11979 (2002).
20. Stamenkovic, V. R., Mun, B. S., Mayrhofer, K. J. J., Ross, P. N. & Markovic, N. M. Effect of surface composition on electronic structure, stability, and electrocatalytic properties of Pt-transition metal alloys: Pt-skin versus Pt-skeleton surfaces. *J. Am. Chem. Soc.* **128**, 8813–8819 (2006).
21. Koh, S. & Strasser, P. Electrocatalysis on bimetallic surfaces: Modifying catalytic reactivity for oxygen reduction by voltammetric surface dealloying. *J. Am. Chem. Soc.* **129**, 12624–12625 (2007).
22. Zhang, J. L., Vukmirovic, M. B., Xu, Y., Mavrikakis, M. & Adzic, R. R. Controlling the catalytic activity of platinum-monolayer electrocatalysts for oxygen reduction with different substrates. *Angew. Chem. Int. Ed.* **44**, 2132–2135 (2005).
23. Mukerjee, S. & Srinivasan, S. Enhanced electrocatalysis of oxygen reduction on platinum alloys in proton-exchange membrane fuel-cells. *J. Electroanal. Chem.* **357**, 201–224 (1993).
24. Toda, T., Igarashi, H., Uchida, H. & Watanabe, M. Enhancement of the electroreduction of oxygen on Pt alloys with Fe, Ni, and Co. *J. Electrochem. Soc.* **146**, 3750–3756 (1999).
25. Mavrikakis, M. Computational methods: A search engine for catalysts. *Nature Mater.* **5**, 847–848 (2006).
26. Mani, P., Srivastava, R. & Strasser, P. Dealloyed Pt–Cu core–shell nanoparticle electrocatalysts for use in PEM fuel cell cathodes. *J. Phys. Chem. C* **112**, 2770–2778 (2008).
27. Wang, C. *et al.* Monodisperse Pt₃Co nanoparticles as a catalyst for the oxygen reduction reaction: Size-dependent activity. *J. Phys. Chem. C* **113**, 19365–19368 (2009).
28. Wang, C. *et al.* Monodisperse Pt₃Co nanoparticles as electrocatalyst: The effects of particle size and pretreatment on electrocatalytic reduction of oxygen. *Phys. Chem. Chem. Phys.* **12**, 6933–6939 (2010).
29. Van der Vliet, D. *et al.* Platinum-alloy nanostructured thin film catalysts for the oxygen reduction reaction. *Electrochim. Acta* **56**, 8695–8699 (2011).
30. Zeis, R., Mathur, A., Fritz, G., Lee, J. & Erlebacher, J. Platinum-plated nanoporous gold: An efficient, low Pt loading electrocatalyst for PEM fuel cells. *J. Power Sources* **165**, 65–72 (2007).
31. Habas, S. E., Lee, H., Radmilovic, V., Somorjai, G. A. & Yang, P. Shaping binary metal nanocrystals through epitaxial seeded growth. *Nature Mater.* **6**, 692–697 (2007).
32. Tao, F. *et al.* Reaction-driven restructuring of Rh–Pd and Pt–Pd core–shell nanoparticles. *Science* **322**, 932–934 (2008).
33. Inaba, M. *et al.* Controlled growth and shape formation of platinum nanoparticles and their electrochemical properties. *Electrochim. Acta* **52**, 1632–1638 (2006).
34. Paulus, U. A. *et al.* Oxygen reduction on carbon-supported Pt–Ni and Pt–Co alloy catalysts. *J. Phys. Chem. B* **106**, 4181–4191 (2002).
35. Antonietti, M. & Ozin, G. A. Promises and problems of mesoscale materials chemistry or why meso? *Chem. Eur. J.* **10**, 28–41 (2004).
36. Mukerjee, S., Srinivasan, S., Soriaga, M. P. & Mcbreen, J. Role of structural and electronic-properties of Pt and Pt alloys on electrocatalysis of oxygen reduction—an *in-situ* XANES and EXAFS investigation. *J. Electrochem. Soc.* **142**, 1409–1422 (1995).
37. Debe, M. K. & Drube, A. R. Structural characteristics of a uniquely nanostructured organic thin-film. *J. Vacuum Sci. Technol. B* **13**, 1236–1241 (1995).
38. Debe, M. K. & Poirier, R. J. Postdeposition growth of a uniquely nanostructured organic film by vacuum annealing. *J. Vacuum Sci. Tech. A* **12**, 2017–2022 (1994).
39. Debe, M. K., Schmoeckel, A. K., Vernstrom, G. D. & Atanasoski, R. High voltage stability of nanostructured thin film catalysts for PEM fuel cells. *J. Power Sources* **161**, 1002–1011 (2006).
40. Debe, M. K. in *Handbook of Fuel Cells – Fundamentals, Technology and Applications* (eds Vielstich, W., Lamm, A. & Gasteiger, H. A.) Ch. 45 (Wiley, 2003).
41. Debe, M. K. *et al.* Extraordinary oxygen reduction activity of Pt₃Ni₇. *J. Electrochem. Soc.* **158**, B910–B918 (2011).

42. Somorjai, G. A. Surface science and catalysis. *Science* **227,** 902–908 (1985).
43. Tao, A. R., Habas, S. & Yang, P. D. Shape control of colloidal metal nanocrystals. *Small* **4,** 310–325 (2008).
44. Lai, S. C. S. & Koper, M. T. M. The influence of surface structure on selectivity in the ethanol electro-oxidation reaction on platinum. *J. Phys. Chem. Lett.* **1,** 1122–1125 (2010).
45. Wadayama, T. *et al.* Oxygen reduction reaction activities of Ni/Pt(111) model catalysts fabricated by molecular beam epitaxy. *Electrochem. Commun.* **12,** 1112–1115 (2010).
46. Gancs, L., Kobayashi, T., Debe, M. K., Atanasoski, R. & Wieckowski, A. Crystallographic characteristics of nanostructured thin-film fuel cell electrocatalysts: A HRTEM study. *Chem. Mater.* **20,** 2444–2454 (2008).
47. Subbaraman, R., Strmcnik, D., Paulikas, A. P., Stamenkovic, V. R. & Markovic, N. M. Oxygen reduction reaction at three-phase interfaces. *Chem. Phys. Chem.* **11,** 2825–2833 (2010).
48. Debe, M. K. *et al.* Nanostructured thin film catalysts for PEM fuel cells by vacuum web coating. (Society of Vacuum Coaters—50th Annual Technical Conference Proceedings, 2007).

Author contributions

D.F.V., C.W. and V.R.S. designed the experiments. C.W., D.F.V., D.T., D.S., X.F.Z., R.T.A., M.K.D. and V.R.S. carried out the experimental work. D.F.V., C.W., M.K.D., N.M.M. and V.R.S. discussed the results and V.R.S. wrote the manuscript.

Additional information

Supplementary information is available in the online version of the paper. Reprints and permissions information is available online at www.nature.com/reprints. Correspondence and requests for materials should be addressed to V.R.S.

Competing financial interests

The authors declare no competing financial interests.